International Journal of Mass Spectrometry 442 (2019) 7–13

Contents lists available at ScienceDirect

International Journal of Mass Spectrometry

journal homepage: www.elsevier.com/locate/ijms

Characterization of ion transmission in UV-FAIMS by incorporating ion recombination

Han Wang [a, b], Youjiang Liu [a], Shan Li [a], Xiaozhi Wang [c], Jiaoyu Deng [d], Chilai Chen [a, *]

[a] State Key Laboratory of Transducer Technology, Hefei Institute of Intelligent Machines, Chinese Academy of Sciences, Hefei, 230031, China
[b] University of Science and Technology of China, Hefei, 230027, China
[c] Department of Information Science and Electronic Engineering, Zhejiang University, Hangzhou, 310027, China
[d] State Key Laboratory of Virology, Wuhan Institute of Virology, Chinese Academy of Sciences, Wuhan, 430071, China

ARTICLE INFO

Article history:
Received 9 November 2018
Received in revised form
17 April 2019
Accepted 17 April 2019
Available online 8 May 2019

Keywords:
High-field asymmetric waveform ion mobility spectrometry
Ion loss
Quantitation
Ion recombination
Recombination loss factor

ABSTRACT

High-field asymmetric waveform ion mobility spectrometry (FAIMS) is a powerful technique for the separation and characterization of gas-phase ions. However, the quantitative model for this technique is incomplete because previous studies on ion loss have mostly focused on ion neutralization and diffusion in the separation process and neglected ion annihilation owing to ion recombination in the transmission process. In this work, an ion recombination model of UV-FAIMS was described and validated using a broad range of experimental gas flow rates (0–800 L/h) and concentrations (10 ppb–100 ppm). The theoretical analysis provided a new solution method for important parameters and indicated the existence of a linear growth interval and a point of saturated signal intensity, both of which were explained by the introduced recombination loss factor and validated experimentally. In particular, the existence of saturation was verified for the first time. Based on this theory, ionization efficiencies of 4.56×10^{-5}, 5.41×10^{-5}, and 4.47×10^{-6} were calculated for 1,3-butadiene, acetone, and ammonia, respectively, at atmospheric pressure, with corresponding the recombination coefficients of 2.56×10^{-7}, 3.74×10^{-7}, and 1.89×10^{-8} cm^3s^{-1}. Further, an optimized quantitative model of UV-FAIMS was proposed by incorporating ion recombination theory, providing the optimum quantitative interval and a parameter optimization method for UV-FAIMS, which were also validated using a wide range of experimental conditions. This work provides a basis for parameter optimization for UV-FAIMS and a new method of determining the ionization efficiency and recombination coefficient of a gas-phase analyte. Furthermore, the incorporation of ion recombination theory is instructive for the construction of quantitative models of atmospheric-pressure photoionization mass spectrometry and UV-ion mobility spectrometry.

1. Introduction

High-field asymmetric waveform ion mobility spectrometry (FAIMS) is an analytical technique for trace gas ions operated at ambient pressure based on the nonlinear variation (alpha dependence, $\alpha(E/N)$) of the ion mobility (K:$cm^2V^{-1}s^{-1}$) under a high electric field. The change in ion mobility with electric field under high electric fields is shown by Eq. (1):

$$K = K_0\left(1 + \alpha\left(\frac{E}{N}\right)\right) = K_0\left[1 + \sum_{n=1}^{\infty} \alpha_{2n}\left(\frac{E}{N}\right)^{2n}\right] \quad (1)$$

where K_0 is the mobility coefficient under low-field condition, E/N is the electric field in Townsend (1 Td = 10^{-17} V cm^2). Under normal conditions ($N_0 = 2.687 \times 10^{19}$ cm^{-3}), 1 Td corresponds to 268.7 Vcm^{-1} and α_2,α_2 … α_{2n} are series coefficients of the alpha dependence expansion (for more details, see Ref. [1]). In the FAIMS method, the alpha dependence is a unique feature of the ions utilized for ion separation. Ions are introduced in a flow of gas that carries them through a narrow gap between two electrodes. Under high frequencies, an asymmetric waveform electric field (dispersion voltage; DV), which acts perpendicular to the direction of gas flow, affects of trajectory of different ion species, which

Abbreviations: FAIMS, high-field asymmetric waveform ion mobility spectrometry; DV, dispersion voltage; CV, compensation voltage; IMS, ion mobility spectrometry; MS, mass spectrometry; VOC, volatile organic compound; ARD, average relative deviation; R_{loss}, Recombination loss factor.

* Corresponding author.
E-mail address: chlchen@iim.ac.cn (C. Chen).

https://doi.org/10.1016/j.ijms.2019.04.008
1387-3806/

consequently may be separated.

FAIMS provides potential portability and unique selectivity because it can be easily integrated and is largely orthogonal to other gas analytical techniques, such as mass spectrometry (MS), gas chromatography, and ion mobility spectrometry (IMS) [2–7]. The first study to use FAIMS was published by Buryakov et al., in 1993 [8]. Years later, works introducing FAIMS as a preseparation device for MS attracted the attention of many researchers [9–13], and it has been widely used in the rapid separation and quantitative analysis of peptides, proteomics, and pharmaceutical compounds. After the September 11 attacks, numerous studies were conducted on FAIMS owing to its potential for detection of explosives [14]. In particular, the works of Eiceman and co-workers, which reduced the complexity of the process and the device size based on micro-electro-mechanical system technology, made portability and on-site detection possible [14–16]. In recent years, FAIMS has been applied to the analysis of a variety of chemicals at trace levels, including explosives, drugs, chemical warfare agents, toxic and industrial components, sulfur-containing chemicals, and other organic and inorganic substances. Notably, vacuum ultraviolet lamps as a soft ionization source have given FAIMS a unique advantage in volatile organic compound (VOC) detection owing to decreased fragmentation [17–20].

Analytical techniques are primarily applied for quantitative analysis, and the most common method used with the FAIMS technique is the experimental calibration method. Suresh et al. proposed the use of UV-FAIMS to measure trace amounts of VOCs, and using acetone, hexane, and an acetone–hexane mixture, a linear range of 1–270 ppm was estimated [17]. Mohsen et al. used a portable FAIMS instrument to detect two families of illicit drugs, with a linear response of 12.5–500 ppb obtained with samples of methamphetamine, amphetamine, and Δ^9-tetrahydrocannabinol [18]. Chen et al. investigated trace amounts of ammonia in water with a homemade UV-FAIMS system, and linearity was observed between 0.55 and 11 ppm [21]. The above works demonstrate the potential of FAIMS for deployment as a portable and quantitative technique in the fields of VOC analysis, public security, and environmental protection. However, as the calibration method relies heavily on experimental conditions and instruments, these results lack universality, stability, and repeatability.

Therefore, the establishment of a quantitative model of FAIMS is an urgent necessity. By simplifying the assumptions for the gas flow rate and the operational boundary conditions, Krylov et al. built a solvable, one-dimensional, time-dependent, mathematical model of FAIMS focused on its analytical parameters and ion properties. This work pioneered theoretical research on FAIMS [1,22,23]. By neglecting ion diffusion and introducing ion trajectory and loss height, Chen et al. proposed a mathematical model of the FAIMS spectral peak profile by considering the structure of the ion drift tube, the analytical parameters, and the parabolic distribution of the flow field. This work provided an expression for the spectral peak profile of FAIMS [19]. To avoid difficult mathematical analyses, researchers instead used simulations to investigate ion loss. Based on the finite-element method, Cumeras et al. modeled the behavior of acetone ions in FAIMS using the COMSOL Multiphysics software. Their work, which focused on the distribution of targeted ions, concluded that the fluid dynamics and electric field were the most significant factors in FAIMS [24]. To optimize the ion transmission efficiency at the FAIMS-MS interface, Prasad et al. developed an algorithm to compute the ion trajectory of hydroxyproline, leucine, hydrated oxygen, 2-propanone, and 2-dodecanone using the Simion software. This work was devoted to simulating ion loss and concluded that the bulk of ion loss was caused by fringe fields [25]. These mathematical analyses and simulations provided intuitive observations of ion distribution and ion trajectory. However, these works focused on ion loss from ion neutralization and diffusion during the separation process and neglected ion recombination loss during the transmission process.

In this study, to explore the ion loss that occurs owing to ion recombination during the transmission process and to build a comprehensive model of FAIMS, the concept of a transmission region and ion recombination theory were introduced. The ion loss during the transport process was investigated by conducting a wide range of experiments while varying different parameters. We expect this work will provide a valuable reference for the quantitative application of FAIMS as well as accurate quantitative analysis using UV-MS [26] and total-quantity analysis using a photoionization detector.

2. Theory

FAIMS optimizations in terms of the separation field and alpha modification have been the subject of previous publications [1,22,23]. These works focused on the FAIMS analytical channel, the influence of instrument parameters on FAIMS performance, and the balance between sensitivity and selectivity, but neglected ion loss during the transmission process, as a lossless transmission was hypothesized. We aim to provide an optimized mathematical model of UV-FAIMS by incorporating a transmission region and ion recombination theory, which is expected to enhance the application of FAIMS to quantitative analysis.

As shown in Fig. 1, sample molecules are ionized in the ionization region, and the input ion concentration (n_{in}: cm^{-3}) mainly depends on the type and concentration of analyte and the type of ionization source. For a predetermined analyte in UV-FAIMS, the ionization efficiency is constant. In addition, the UV source guarantees outstanding linearity between the analyte concentration and the ion concentration over a concentration range of several ppt to hundreds of ppm [27–29]. Thus, the input ion concentration can be expressed as:

$$n_{in} = \mu_0 C \tag{2}$$

Where μ_0 is the ionization efficiency of the analyte, and C (cm^{-3}) is the analyte concentration.

The ions are drawn through the analytical channel by the gas flow, and ion recombination plays an import role in ion loss, which has been neglected in previous research. Below, we use the following terms and definitions: K ($cm^2V^{-1}s^{-1}$) and D (cm^2s^{-1}) are the ion mobility and diffusion, respectively; H (pA) is the FAIMS peak height; $h = 0.5$ mm, $l = 32$ mm, and w = 8 mm are the height, length, and width of the FAIMS analytical channel in this work; $A = h$w is the cross-sectional area of the analytical channel; Q (cm^3s^{-1}) is the drift gas flow rate; e is the base of the natural logarithm; and g (mm) is the effective gap.

Ion recombination can be expressed by Refs. [30,31]:

$$n_{\text{out}} = \frac{n_{\text{in}}}{1 + k_{rec} n_{\text{in}}} \tag{3}$$

where n_{out} is the ion flux at the output of the analytical channel and n_{in} is the total ion flux at the input of the analytical channel, k_{rec} (m^3s^{-1}) is recombination coefficient, determined by the type of substance, and $t_{res} = lhw/Q = lA/Q$ (ms) is the drift time of ions in the transmission process.

From Eqs. (2) and (3), we have:

$$n_{out} = \frac{n_{in}}{1 + k_{rec} n_{\text{in}}} = \frac{\mu_0 C}{1 + k_{rec}\frac{lA}{Q}\mu_0 C} = \frac{1}{\frac{1}{\mu_0 C} + k_{rec}\frac{lA}{Q}} \tag{4}$$

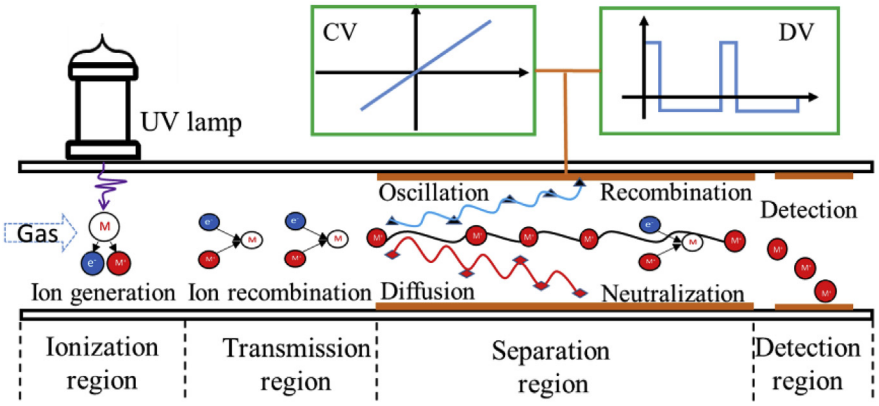

Fig. 1. Schematic of the FAIMS system.

To present results easier and clearer, a dimensionless flowrate is defined and named recombination loss factor as:

$$R_{loss} = \frac{Q}{k_{rec} l A \mu_0 C} \tag{5}$$

With R_{loss}, equation (4) is written as:

$$n_{out} = \frac{\mu_0 C}{1 + R_{loss}^{-1}} \tag{6}$$

When R_{loss} is large, means $Q \gg k_{rec} l A \mu_0 C$, C plays dominate role on n_{out}, giving:

$$n_{out} \approx \frac{1}{1/\mu_0 C} = \mu_0 C \tag{7}$$

In this case, $n_{out} \propto C$. In others words, the signal intensity (I) is completely determined by the sample concentration and is independent of the flow rate (Q). Further, Eq. (7) provides an easy way to obtain the ionization efficiency μ_0 experimentally.

When R_{loss} is small, means $Q \ll k_{rec} l A \mu_0 C$, Q plays dominate role on n_{out}, giving:

$$n_{out} \approx \frac{1}{k_{rec} A l / Q} = \frac{Q}{k_{rec} A l} \tag{8}$$

In this case, for a predetermined analytical channel, $n_{out} \propto Q$. In others words, the carrier gas flow plays a dominant role in the signal intensity, resulting in a serious ion recombination effect, and a slight change in Q will have an obvious impact on the signal intensity. Further, Eq. (8) provides an easy way to obtain the recombination coefficient k_{rec} experimentally.

For planar FAIMS, in the separation process, ion diffusion and neutralization play dominant roles in ion loss and the ion transmission coefficient (L), which is the ratio between the ion fluxes at the input and the output of the analytical channel, is given by Eq. (9):

$$L = \exp\left(- t_{res} \frac{\pi^2 D}{g^2} \right) \tag{9}$$

The effective gap g, between the electrodes is smaller than the physical gap because the ions need enough space to oscillate with the DV without striking the electrodes (for more details, see Ref. [1]). The concept of ion transmission through the filter gap is used to calculate the FAIMS peak height (H). Here, we try to optimize the model of FAIMS by incorporating ion recombination theory. Combining Eq. (4) with Eq. (9), the FAIMS peak height is given by:

$$H = \frac{\mu_0 C}{1 + k_{rec} \frac{lA}{Q} \mu_0 C} \exp\left(- t_{res} \frac{\pi^2 D}{g^2} \right) = \frac{\mu_0 C}{1 + B^{-1}} \exp\left(- t_{res} \frac{\pi^2 D}{g^2} \right) \tag{10}$$

When R_{loss} is small, means $\frac{Q}{C} \ll k_{rec} l A \mu_0$,

$$H = \frac{Q}{k_{rec} A l} \exp\left(- \frac{Al}{Q} \frac{\pi^2 D}{g^2} \right) = n_x Q \exp\left(- \frac{Al}{Q} \frac{\pi^2 D}{g^2} \right) \tag{11}$$

Where $n_x = 1/k_{rec} A l$. In this case, this model has the same form as Krylov' mathematical model of FAIMS [1,22,23]. Here, $H \propto Q$ and the carrier gas plays a dominant role in the signal intensity, resulting in a serious ion recombination effect, and a slight change in Q will have an obvious impact on the signal intensity.

When R_{loss} is large, means $\frac{Q}{C} \gg k_{rec} l A \mu_0$,

$$H = \mu_0 C \exp\left(- \frac{Al}{Q} \frac{\pi^2 D}{g^2} \right) \tag{12}$$

In this case, ion neutralization and diffusion play a dominant role in the signal intensity, and the effects of ion recombination can be neglected. Thus, a change in Q will have little effect on the signal intensity, which is very useful for quantitative analysis, as the accurate control of electrical signals is much simpler than the accurate control of gas flow.

3. Experimental

The experimental system is shown in Fig. 2. Gaseous samples (purity > 99.95%) and the carrier gas (N_2) were provided by Nanjing Shangyuan Industrial Gas Co., Ltd. (Jiangsu, China). The flow meter with specifications of 0–1000 L/h ensured a wide range of adjustable conditions. The signal was collected using a data acquisition card (NI USB-6009, National Instruments Corp.) connected to the LabVIEW software to show the FAIMS data in real time. Some important FAIMS parameters are shown as follows: Ionization source is UV lamp (10.6 eV), DV (V) changes in 0–1500 V, CV (V) changes in −30 to +30 V, sample components are N2 and gaseous sample (99.95%).

4. Results and discussion

4.1. Verification of ion recombination loss

Ion recombination theory predicts that when $Q \ll k_{rec} l A \mu_0 C$, the

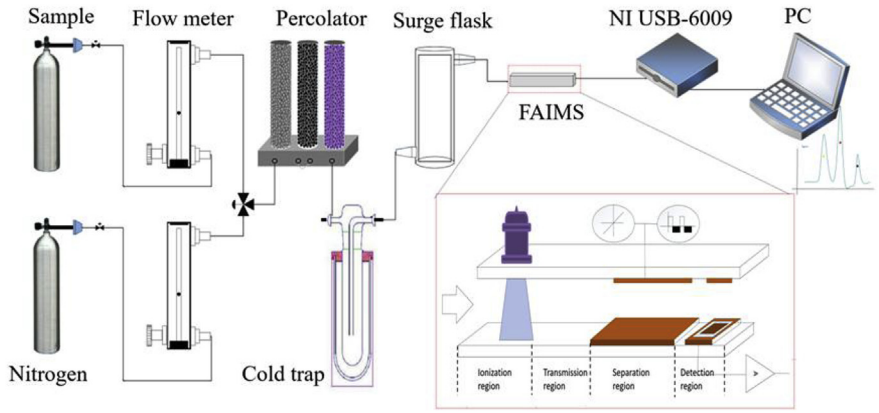

Fig. 2. Schematic diagram of the experimental system.

signal intensity is proportional to the gas flow rate with a slope of $\frac{1}{k_{rec}l}$, but when $Q \gg k_{rec}lA\mu_0 C$, the signal intensity is proportional to the concentration of analyte and independent of the gas flow rate, with a slope of μ_0. This theory also predicts the existence of a saturated signal intensity (I_s) that is dependent on the residence time (Q, *l*, and A), the ionization efficiency of the analyte μ_0, and the analyte concentration *C*. To validate our theoretical model, we examined the ion loss occurring in a homemade FAIMS instrument over a broad range of gas flow rates (Q) and concentrations (C).

The factors that influence ion recombination were examined experimentally by changing the gas flow rate from 0 to 800 L/h and the concentration from 10 ppb to 100 ppm using ammonia, acetone, and 1,3-butadiene samples. Practically, a special experimental setup and circuit connection (Fig. 3) was designed to eliminate the effects of ion neutralization and diffusion, allowing the effects of ion recombination during ion transport to be investigated systematically.

The experimental results for ion loss during the transmission process and the factors that influence this process are discussed here. First, samples of 10 ppm 1,3-butadiene, acetone, and ammonia were investigated, with both DV and CV acting as grounded. The plots of the signal intensity (I) and the normalized signal intensity (I_n) against the gas flow rate are shown in Fig. 4. When Q was changed in the range of 0–100 L/h, the signal intensity increased linearly with the increasing gas flow rate. However, at

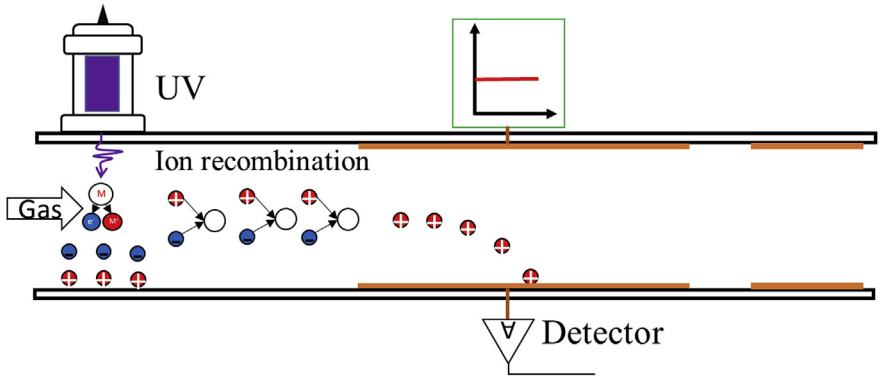

Fig. 3. Experimental setup and circuit connection.

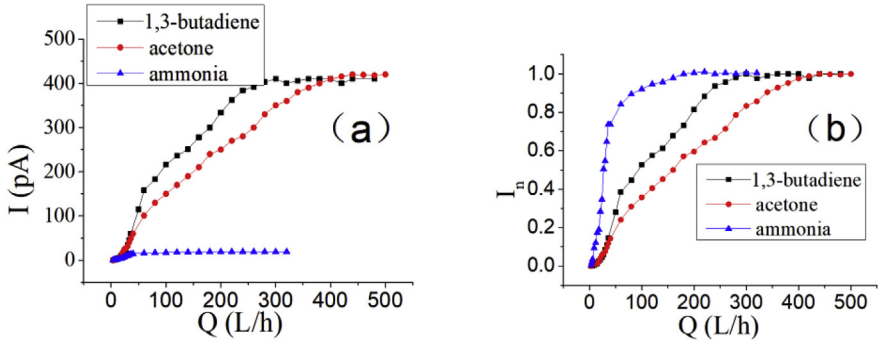

Fig. 4. Dependence of signal intensity on the gas flow rate for samples of 10 ppm 1,3-butadiene, acetone, and ammonia. Signal intensity (a) and normalized signal intensity (b) plotted against the gas flow rate.

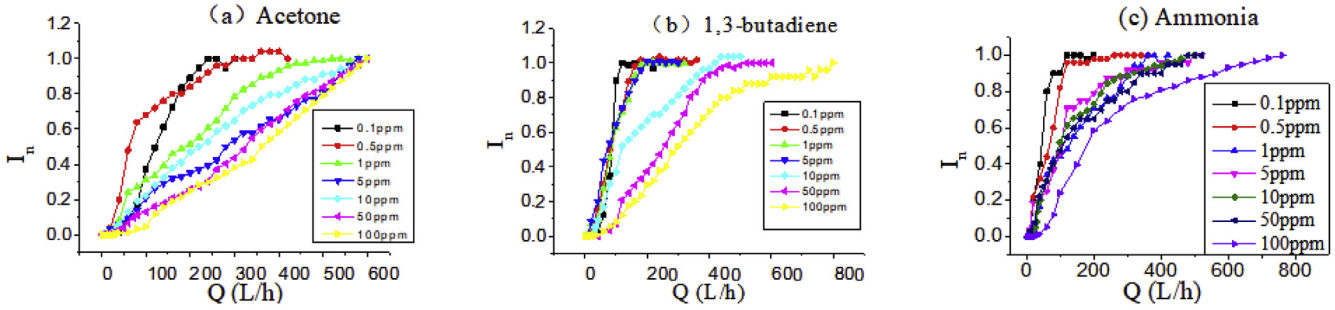

Fig. 5. Dependence of signal intensity on gas flow rate at various concentrations of acetone (a), 1,3-butadiene (b), and ammonia (c).

higher Q, the growth rate of the signal intensity gradually decreased and finally reached saturation, with the saturated signal intensity strongly depending on the analyte type. The saturated gas flow rates (Q_s) were 320, 340, and 200 L/h and the I_s values were 410, 420, and 19.1 pA for 1,3-butadiene, acetone, and ammonia, respectively.

Investigation of the effect of the analyte concentration (C) on ion loss during the transmission process (Fig. 5) showed the same trend as observed for the gas flow rate. In addition, it was found that the saturated signal intensity also strongly depended on analyte concentration. For the same analyte, the growth rate of the relative signal intensity decreased at higher concentrations. In addition, saturation became more difficult at higher concentrations. A comparison of the different analytes revealed that saturation of ammonia was easier than that of 1,3-butadiene or acetone.

The above experimental results confirmed the existence of a saturated signal intensity (I_s) for the first time, as well as the effects of t_{res}, μ_0, and C on ion loss, providing direct verification of the ion recombination loss theory of UV-FAIMS proposed in this work.

The experimental data was further analyzed to verify Eqs. (7)–(9) and calculate the ionization efficiency μ_0 and recombination coefficient k_{rec}.

1) When $Q \gg k_{rec} l A \mu_0 C$

As shown in Figs. 4 and 5, the signal intensity was independent of the gas flow rate when Q was sufficiently high, which is in agreement with Eq. (7). To further analysis the relationship between concentration and signal intensity, the signal intensity was plotted against the concentration of 1,3-butadiene at various gas flow rates (Fig. 6a). All the curves were fitted linearly, and the Pearson correlation coefficient (Pearson's r) was chosen to represent the linearity (Fig. 6b). The Pearson's r increased from 0.867 at a Q of 20 L/h to 0.991 at a Q of 500 L/h, where Q increases to Q_s for various concentrations. This law showed that the analyte concentration only exhibited a good linear relationship with the signal intensity when the gas flow rate was high enough (>Q_s). Plots of C against I_s are shown in Fig. 6c for different analytes. All the curves were fitted linearly, with Pearson's r values of 0.9991, 0.9999, and 0.9999 and slopes of 27.0, 32.1, and 12.5 for 1,3-butadiene, acetone,

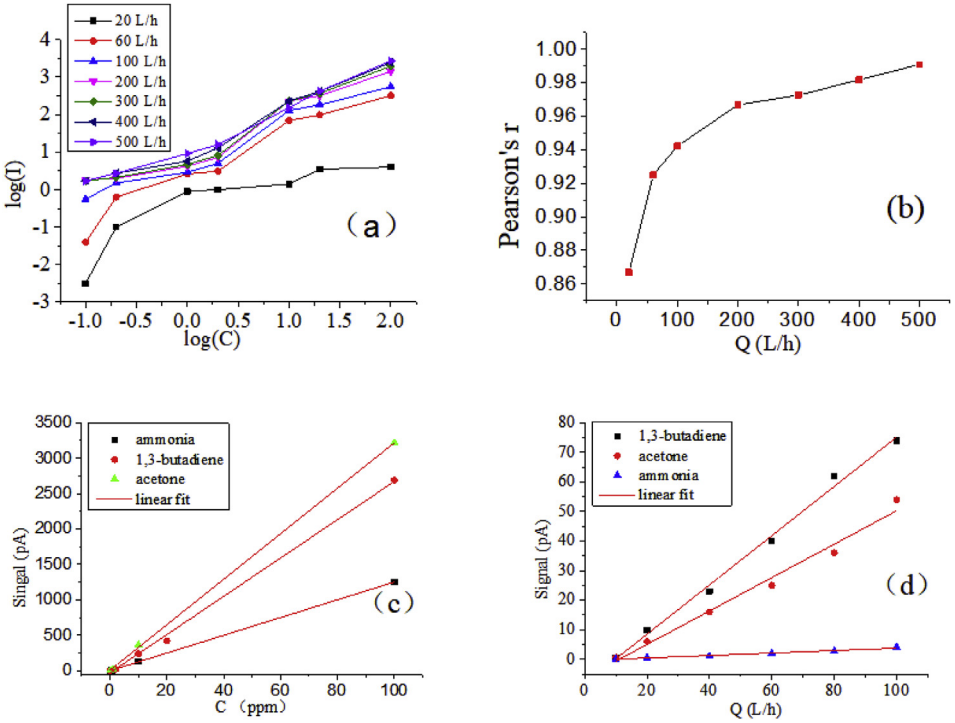

Fig. 6. Relationship between the signal intensity and the concentration of 1,3-butadiene (a) and the corresponding linearity (b) at various gas flow rates. Relationship between the saturated signal intensity and the concentration of different analytes (c). Relationship between the signal intensity and the gas flow rate in the range 0–100 L/h (d).

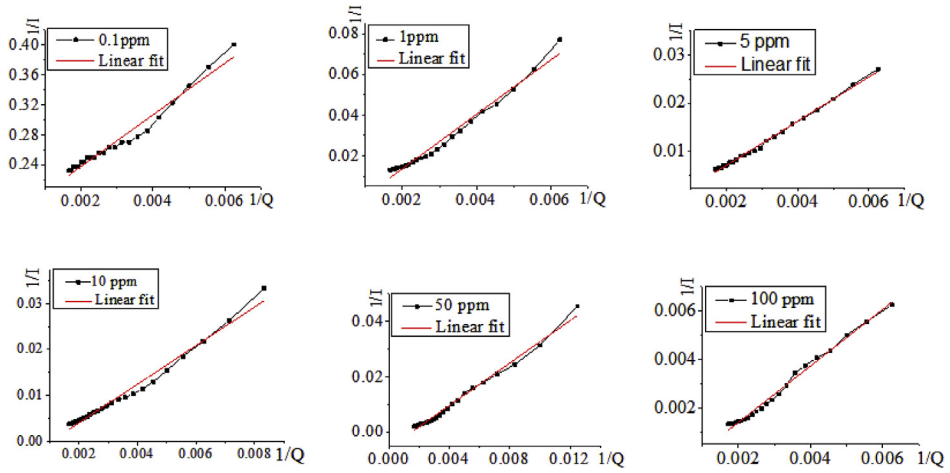

Fig. 7. Dependence of ion recombination on the gas flow rate of 1,3-butadiene.

and ammonia, respectively. These plots exhibited good linearity, which is a good evidence for the validity of Eq. (7). Further, the ionization efficiencies were calculated to be 4.56×10^{-5}, 5.41×10^{-5} and 4.47×10^{-6} for 1,3-butadiene, acetone, and ammonia, respectively.

2) When $Q \ll k_{rec} l A \mu_0 C$

The plots of the signal intensity against the gas flow rate in the range 0–100 L/h were extracted (Fig. 6d). All the curves were fitted linearly, with Pearson's r values of 0.992, 0.997, and 0.993 and slopes of 0.565, 0.833, and 0.042 for 1,3-butadiene, acetone, and ammonia, respectively. Thus, the experimental results were in satisfactory agreement with Eq. (8). Further, the recombination coefficients k_{rec} were calculated from the slope to be 2.56×10^{-7}, 3.74×10^{-7} and 1.89×10^{-8} $cm^3 s^{-1}$ for 1,3-butadiene, acetone, and ammonia, respectively. k_{rec} also can be determined easier from a point of R_{loss}, such as $R_{loss} = 1$, the calculated results were 2.55×10^{-7}, 3.72×10^{-7}, and 1.89×10^{-8} $cm^3 s^{-1}$.

3) General situation

Eq. (4) can be further transformed to give:

$$\frac{1}{n_{out}} = \frac{1}{\mu_0}\cdot\frac{1}{C} + k_{rec} l A \frac{1}{Q} = a_0 \frac{1}{C} + a_1 \frac{1}{Q} \tag{13}$$

where $a_0 = {}^1/_{\mu_0}$ and $a_1 = k_{rec} A l$. Thus, for a specific C and analytical channel, $\frac{1}{n_{out}} \propto \frac{1}{Q}$.

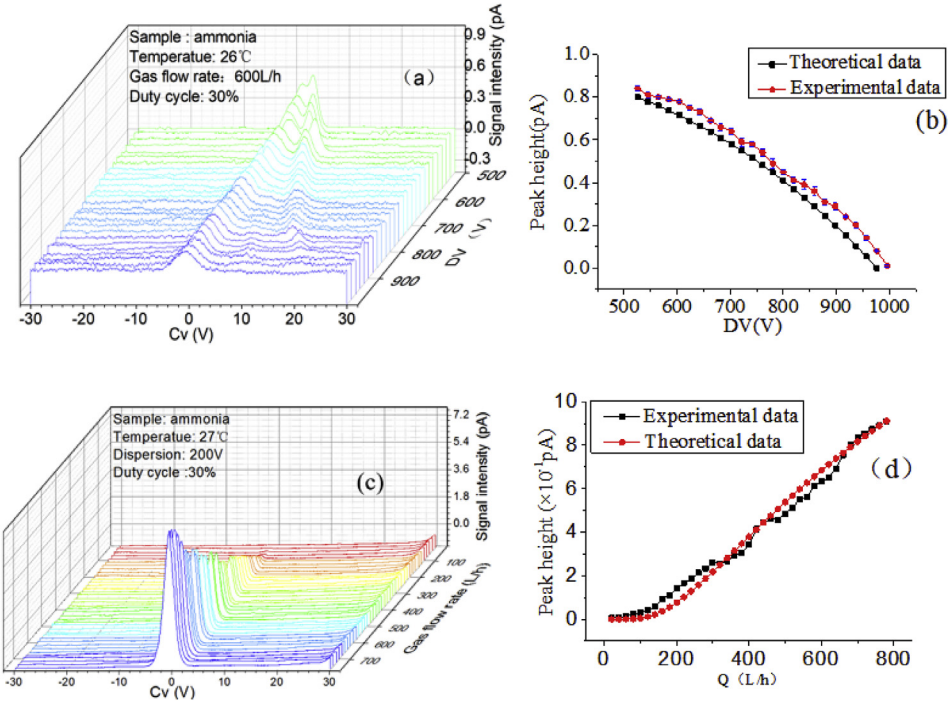

Fig. 8. Validity tests for the developed model. Experimentally collected spectra (a and c) and comparisons between experimental and theoretical data at different DV values (b) and gas flow rates (d).

The reciprocal of the signal intensity of 1,3-butadiene depended linearly on the reciprocal of Q (120–500 L/h) (Fig. 7), which agrees with Eq. (13).

4.2. Verification of the quantitative model

Experiments to confirm the quantitative model were conducted to verify the optimized mathematical model. Using the experimental setup and circuit connection shown in Fig. 1, a compensation voltage (CV) was automatically scanning from −30 to +30 V while Q and DV were varied separately. The resulting signal intensity was detected in the detection region, where a high-field rectangular asymmetric waveform voltage with an amplitude in the range 0–1500 V and a duty cycle of 30% was used as the DV. The correlation between the theoretical curves and the experimental data was used to test the model's validity.

Firstly, the DV was examined using ammonia at a mixing ratio of 0.5 ppm. As shown by Eq. (12), it is easier to verify the effect of the DV on the quantitative analysis using a gas flow rate higher than Q_s. In this case, the gas flow rate was maintained at 600 L/h, which is higher than Q_s, and the DV was increased from 500 to 1000 V in 20 V intervals, and all the collected spectra are shown in Fig. 8a. As shown by the comparison between the experimental and theoretical data at different DV values in Fig. 8b, the experimental peak heights showed good consistency with the theoretical data.

Secondly, we examined the gas flow rate at a DV of 200 V using ammonia at a mixing ratio of 0.5 ppm. The gas flow rate was varied from 0 to 780 L/h, and all the collected spectra are shown in Fig. 8c. A comparison between the theoretical and experimental data (Fig. 8d) shows excellent agreement over a wide range, which directly validates the proposed quantitative model in Eq. (10).

5. Conclusion

A theoretical analysis of ion recombination in UV-FAIMS provided a new method for determining the ionization efficiency and recombination coefficient of gas-phase ions. Furthermore, this approach provided a mathematical expression for ion recombination loss during the transmission process, which was validated experimentally. An optimized mathematical model of UV-FAIMS was proposed based on ion recombination theory, and the accuracy of this wide-range quantitative model was verified using ammonia. This work provides a reference for parameter optimization and widespread quantitative analysis using UV-FAIMS, and further research will focus on building quantitative models of UV-IMS and atmospheric-pressure photoionization mass spectrometry by incorporating ion recombination.

Funding

This research was supported by the National Key R&D Program of China (2016YFC0201102), the National Natural Science Foundation of China (61871367), the Youth Innovation Promotion Association of the Chinese Academy of Sciences (2013213), and the National Natural Science Foundation of China (41805017).

Declarations of interest

None.

References

[1] E.V. Krylov, E.G. Nazarov, R.A. Miller, Int. J. Mass Spectrom. 266 (2007) 76–85.
[2] B.M. Kolakowski, Z. Mester, Analyst 132 (2007) 842–864.
[3] R. Cumeras, E. Figueras, C.E. Davis, J.I. Baumbach, I. Gràcia, Analyst 140 (2015) 1376–1390.
[4] R. Cumeras, E. Figueras, C.E. Davis, J.I. Baumbach, I. Gràcia, Analyst 140 (2015) 1391–1410.
[5] P. Hatsis, J.T. Kapron, Rapid Commun. Mass Spectrom. 22 (2008) 735–738.
[6] D.A. Barnett, B. Ells, R. Guevremont, R.W. Purves, J. Am. Soc. Mass Spectrom. 10 (1999) 1279–1284.
[7] X. Li, G. Jiang, C. Luo, F. Xu, Y. Wang, L. Ding, C.-F. Ding, Anal. Chem. 81 (2009) 4840–4846.
[8] I.A. Buryakov, E.V. Krylov, E.G. Nazarov, U.K. Rasulev, Int. J. Mass Spectrom. Ion Process. 128 (1993) 143–148.
[9] R. Guevremont, D.A. Barnett, R.W. Purves, J. Vandermey, Anal. Chem. 72 (2000) 4577–4584.
[10] R. Guevremont, D.A. Barnett, R.W. Purves, L.A. Viehland, J. Chem. Phys. 114 (2001) 10270–10277.
[11] R. Guevremont, R.W. Purves, J. Am. Soc. Mass Spectrom. 10 (1999) 492–501.
[12] R. Guevremont, R.W. Purves, Rev. Sci. Instrum. 70 (1999) 1370–1383.
[13] B. Ells, K. Froese, S.E. Hrudey, R.W. Purves, R. Guevremont, D.A. Barnett, Rapid Commun. Mass Spectrom. 14 (2000) 1538–1542.
[14] R.G. Ewing, D.A. Atkinson, G.A. Eiceman, G.J. Ewing, Talanta 54 (2001) 515–529.
[15] R.A. Miller, E.G. Nazarov, G.A. Eiceman, A.T. King, Sensor Actuator Phys. 91 (2001) 301–312.
[16] R.A. Miller, G.A. Eiceman, E.G. Nazarov, A.T. King, Sensor. Actuator. B Chem. 67 (2000) 300–306.
[17] M. Suresh, N.J. Vasa, V. Agarwal, J. Chandapillai, Sensor. Actuator. B Chem. 195 (2014) 44–51.
[18] Y. Mohsen, N. Gharbi, A. Lenouvel, C. Guignard, Procedia Eng. 87 (2014) 536–539.
[19] C. Chen, D. Kong, X. Wang, H. Wang, F. Shuang, T. Mei, Chin. J. Chem. Phys. 24 (2011) 325–329.
[20] A. Agapiou, A. Amann, P. Mochalski, M. Statheropoulos, C.L.P. Thomas, Trac. Trends Anal. Chem. 66 (2015) 158–175.
[21] L.I. Shan, C.L. Chen, D.Q. Zhu, K. Guan, R. Zhi-Ming, Y.J. Liu, Y.U. Jian-Wen, X.U. Qing, Chin. J. Anal. Chem. 66 (2016) 1679–1685.
[22] E.V. Krylov, Int. J. Mass Spectrom. 225 (2003) 39–51.
[23] E. Krylov, Int. J. Ion Mobil. Spectrom. 15 (2012) 85–90.
[24] R. Cumeras, I. Gracia, P. Ivanov, N. Sabate, C. Cane, in: Proceedings of the 2009 Spanish Conference on Electron Devices, 2009, pp. 323–326.
[25] S. Prasad, K. Tang, D. Manura, D. Papanastasiou, R.D. Smith, Anal. Chem. 81 (2009) 8749–8757.
[26] Y. Pan, Y. Hu, J. Wang, L. Ye, C. Liu, Z. Zhu, Anal. Chem. 85 (2013) 11993–12001.
[27] G. Walendzik, J.I. Baumbach, D. Klockow, Anal. Bioanal. Chem. 382 (2005) 1842–1847.
[28] S. Senkan, S. Ozturk, K. Krantz, I. Onal, Appl. Catal. Gen. 254 (2003) 97–106.
[29] S.I. Levikov, J. Appl. Spectrosc. 3 (1965) 355–367.
[30] K. Lehtipalo, M. Sipilä, I. Riipinen, T. Nieminen, M. Kulmala, Atmos. Chem. Phys. 9 (2009) 4177–4184.
[31] R.W. Purves, J. Am. Soc. Mass Spectrom. 21 (2010). R3-R3.